Control of Multiple Heterogeneous Magnetic Micro-Robots in Two Dimensions on Non-Specialized Surfaces

Eric Diller, *Student Member, IEEE,* Steven Floyd, *Member, IEEE,* Chytra Pawashe, and Metin Sitti, *Senior Member, IEEE*

***Abstract*—In this work, we propose methods for controlling multiple untethered magnetic micro-robots (called Mag-μBots), with all dimensions under 1 mm, without the need for a specialized surface. We investigate sets of Mag-μBots that are geometrically designed to respond uniquely to the same applied magnetic fields. By controlling the magnetic field waveforms, individual and sub-groups of Mag-μBots are able to locomote in a parallel but dissimilar fashion. The control of geometrically dissimilar Mag-μBots and a group of identically-fabricated Mag-μBots are investigated, and control strategies are developed for 1D and 2D motion. This is accomplished by learning the velocity response of each micro-robot to various control signals, and using the uniqueness of each micro-robot response to achieve independent control. The effect of high-level control parameters are investigated in simulation and experiment, and the simultaneous independent global positioning of two and three micro-robots is demonstrated in two-dimensional space. As this control method is accomplished without the use of a specialized surface, it has potential applications in areas such as micro-fluidic systems and bio-manipulation.**

***Index Terms*—Micro/Nano Robots, Distributed Robot Systems, Parallel Robots**

I. Introduction

THE emergence of sub-millimeter sized micro-robots has brought with it new approaches to power delivery and control at the micro-scale. The current designs in literature, including electrostatic [1], [2], electromagnetic [3]–[7], optical [8], thermal [9], chemical [10], and bacteria propelled systems [11], [12], have demonstrated wireless motion control of individual mobile micro-robots.

One significant challenge in micro-robotics is the simultaneous control of multiple untethered agents. This is difficult with current micro-robotic systems because driving signals are typically uniform in the workspace, so all agents receive identical control inputs. Methods to address individual micro-robots must be developed for the full control of multiple micro-robots.

Using electrostatic actuation, Donald *et al.* [1] have controlled up to four micro-robots in parallel by designing individuals to be mechanically unique so that they respond differently to global driving fields generated by the structured substrate. They have established a set of control signals that causes individuals to either turn in circles or translate. Using five such control signals, they can command between zero and four of the robots to turn. In this way, a library of motion primitives has been created, and by using sophisticated algorithms, paths are designed to move the four micro-robots from initial to final configurations. Because of the need for 'stationary' individuals to turn repeatedly in circles, this methodology imposes limits on the amount of free space each individual micro-robot requires and limits the performance of the system.

Using resonant magnetic micro-robots, Nelson *et al.* [3], [13] have demonstrated that decoupled motion is possible with two mechanically unique micro-robots possessing different resonant frequencies; the frequency of the driving magnetic field is varied to select each micro-robot. Similar to [1], these individual micro-robots must be physically unique so that their responses to the global driving magnetic fields differ. By using devices with highly different resonant frequencies, control is serial, and time multiplexing of the driving signals must be used to achieve the appearance of simultaneous motion control. While individual devices of this type have been reported to operate on unstructured surfaces such as a clean silicon wafer, all demonstrated multi-robot operation has been done using a structured substrate that generates electrostatic fields. The authors report that this requirement is due to drifting and backwards motion that can occur when not using such a surface. However, in principle, this resonant frequency method could be used to control multiple micro-robots without a specialized surface, once these undesired behaviors have been understood and accounted for.

Using a simulation of holonomically-constrained micro-robots [14], high levels of controllability of a number of micro-robots with limited control inputs has been demonstrated. In this work, the velocity of each micro-robot (modelled after those in [1]) is directed forward in the local coordinate frame of each micro-robot, allowing for arbitrary final positions to be achieved even though all agents receive the same control signals. However, this work was never implemented in a real system.

In previous work [15], we have introduced methods to independently address multiple magnetic micro-robots (Mag-μBots) without the need for a specialized surface. Individual Mag-μBots themselves can operate on arbitrary substrates such as the surface of a U.S. dime, as well as in gaseous and liquid environments [6]. To address multiple agents, the micro-robots are designed to respond uniquely to the global driving magnetic fields, similar to [1], [3]. This work studied the physics of heterogeneous motion control using several selection methods, and demonstrated that selective control is possible.

In this work, we use a single selection method from [15] to

E. Diller and M. Sitti are with the Department of Mechanical Engineering, Carnegie Mellon University, Pittsburgh, PA 15213, USA sitti@andrew.cmu.edu

S. Floyd was with the Department of Mechanical Engineering, Carnegie Mellon University. He is now a staff engineer with Areté Associates, Arlington, VA 22202, USA.

C. Pawashe was with the Department of Mechanical Engineering, Carnegie Mellon University. He is now at Intel Corporation, Hillsboro, OR, USA.

This paper has supplementary downloadable material available. This includes three movie clips, which show experimental results of micro-robot motion.

control heterogeneous teams of Mag-μBots along paths in two dimensions. We show that decoupled movement of all micro-robots is not necessary to achieve control over the set in two dimensions, allowing positioning and limited path following of several micro-robots to be achieved and analyzed. The effects of high-level control parameters are investigated and optimized to achieve fast positioning of teams of micro-robots. This work is an extension of [16], providing additional analysis and experimental results.

Without the need for a specialized surface, the proposed approach can allow multiple Mag-μBots to operate in environments that are not conducive to such a surface. For example, specialized electrostatic surfaces as in [1], [3], [17], [18] cannot be effectively operated in ionic environments, such as in fluids that support biological organisms. Bypassing this limitation will allow the proposed approach to be used in a wider range of environments, and enable applications such as bio-manipulation with multiple micro-robots working in tandem. In addition, the freedom to work in arbitrary environments will allow teams of Mag-μBots to be used in pre-existing areas such as microfluidic channels. Additionally, smaller, slower versions of Mag-μBots will be able to enter very narrow channels and even interact with biological organisms.

While the path following capabilities of teams of Mag-μBots are shown to be limited due to the coupled nature of the method, the ability to position multiple micro-robots accurately has many possible microfluidic applications including valving, mixing, non-contact manipulation, remote sensing and drug delivery for properly scaled micro-robots. Indeed, it is shown that the robot can follow a path within a certain small error (about one robot body-length), which would be adequate for path planning and obstacle avoidance in complex environments.

The paper is organized as follows. Section II introduces a new experimental setup used to operate Mag-μBots. Section III provides a short overview of the physics of independent control of multiple micro-robots. Section IV describes how differences in the velocity response of each micro-robot can be used to command them to arbitrary goal positions in one or two dimensions. Section V presents experiments on one to four heterogeneous micro-robots to analyze the effects of high-level control parameters. The paper is concluded in section VI.

II. Experimental Setup

Mag-μBots are actuated by six independent air-core electromagnetic coils (shown in Fig. 1), aligned to the faces of a cube approximately 8.2 cm on a side. The currents in the electromagnetic coils are controlled using a PC with data acquisition system at a control bandwidth of 10 kHz, using linear electronic amplifiers (SyRen 25, Dimension Engineering Inc.) and Hall-effect current sensors (ACS714, Allegro Microsystems Inc.). Imaging of the Mag-μBots and workspace is accomplished by a CCD camera (Foculus F0134SB) connected to a variable magnification microscope lens, providing up to a 26 mm×20 mm field of view. Magnetic flux densities and gradients of up to 15 mT and 0.65 T m^{-1}, respectively, can be generated in the workspace. For a 20 mm×20 mm workspace in the center of the coil system, the field and field gradient measured with a Hall effect sensor (Allegro 1321) is found to be uniform within 6.0% of the nominal value.

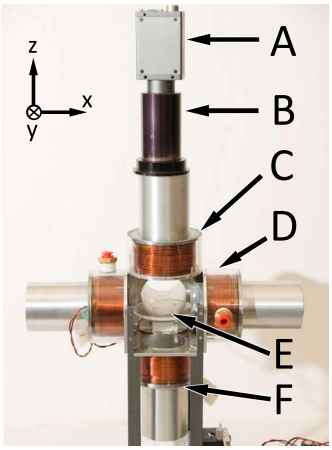

Fig. 1. Photograph of the electromagnetic coil setup. A: camera for top-view vision feedback, B: microscope lens, C: top $+z$ coil, D: $+x$ coil (one of four horizontal coils), E: experiment workspace, and F: bottom $-z$ coil. The $-y$ coil is removed to allow viewing of the workspace.

Mag-μBot actuation is accomplished by the application of magnetic torques and forces, discussed in detail in [6]. Using a number of coils (C, D and F in Fig. 1), magnetic fields and gradients are generated in the robot's workspace (E in Fig. 1). A static magnetic force exerted by the coils on a Mag-μBot is insufficient to translate it due to high friction with and adhesion to the surface. Therefore, the z-directed coils are pulsed using a sawtooth waveform, causing a rocking motion in the Mag-μBot about a horizontal axis perpendicular to the direction of travel. During the sharp change in magnetic field direction due to the sawtooth waveform, the Mag-μBot momentarily slips on the surface due to its high angular velocity; this results in controllable stick-slip motion across the surface. As will be seen in later sections, the velocity response of the Mag-μBot is highly dependent on its physical and magnetic properties, as well as the driving magnetic fields.

In this work, individual Mag-μBots are fabricated to be magnetically hard, retaining their internal magnetization in the absence of an externally applied magnetic field. Mag-μBots are fabricated in a batch process using molding techniques in a manner similar to [19]. Mag-μBots are composed of neodymium-iron-boron (NdFeB) particles in a polyurethane matrix, with fabrication details given in [6]. The molding process is prone to variations in robot geometry (up to $\sim 15\%$ from nominal), but we will show that this does not negatively effect the proposed control method.

III. Modeling Heterogeneous Micro-Robots

Actuated by external magnetic fields, a Mag-μBot will potentially experience electromagnetic, gravitational, adhesive, frictional, and fluid forces applied from the environment. The effects of these forces are explained in detail in [6], [20]. This section provides a brief derivation of the relevant forces and torques, and summarizes the conditions necessary for selective actuation of unique Mag-μBots.

The magnetic torque $\boldsymbol{T}_m$ acting on a Mag-μBot is a function of its magnetic moment $\boldsymbol{m} = V_m \boldsymbol{M}$, and the applied magnetic flux density $\boldsymbol{B}$:

$$\boldsymbol{T}_m = \boldsymbol{m} \times \boldsymbol{B} = V_m \boldsymbol{M} \times \boldsymbol{B} \tag{1}$$

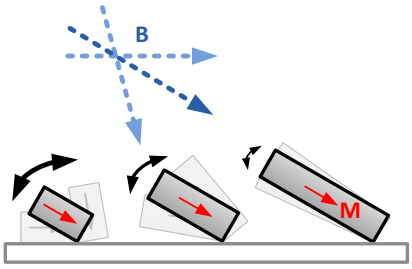

Fig. 2. Schematic of three Mag-μBots of similar magnetizations whose size causes them to behave differently within applied magnetic fields. Longer Mag-μBots have higher rotational inertia and hence lower angular acceleration and smaller total angular swing. The oscillating magnetic field $\boldsymbol{B}$ is shown.

where V_m is the volume of the Mag-μBot and $\boldsymbol{M}$ is the effective magnetization vector.

While magnetic forces arising from field gradients do play a part in the motion of the Mag-μBots, their effects at this scale relative to those from magnetic torques are very small, and so are neglected in these analyses [21].

The gravitational torque, $\boldsymbol{T}_g$, acting about the contact point to hold a Mag-μBot flat on the surface is defined as

$$\boldsymbol{T}_g = (\rho - \rho_{\text{fluid}}) V_m g \frac{L}{2} \hat{\boldsymbol{j}} \tag{2}$$

where ρ is the Mag-μBot density, ρ_{fluid} is the density of the fluid environment, g is the acceleration due to gravity, L is the length of the Mag-μBot and $\hat{\boldsymbol{j}}$ is a unit vector parallel to the surface and perpendicular to $\boldsymbol{M}$.

One method to select multiple Mag-μBots involves utilizing the vibrational response of Mag-μBots of different sizes, which vary due to differing rotational inertias. While we focus on this selection method in this work, additional methods for selecting multiple micro-robots (such as selection by internal magnetization and by shape demagnetization factor for magnetically soft robots) are discussed in [15].

The stick-slip motion used to actuate Mag-μBots is composed of periods of both low and high angular velocities and accelerations. By using a sawtooth magnetic field waveform, the angular rotation during the slip phase is maximized. When the angular velocity is low, the Mag-μBot's center of mass will translate as it rocks on it's point of contact with the surface. When the angular velocity is high, the point of contact will slip while the center of mass remains relatively stationary.

Angular acceleration, $\ddot{\theta}$, is dependent upon the total torque on the Mag-μBot and its rotational inertia J as

$$\ddot{\theta} \propto \frac{|\boldsymbol{T}_m + \boldsymbol{T}_g|}{J} = \frac{|\boldsymbol{T}_m + \boldsymbol{T}_g|}{\frac{1}{12}\rho V_m (L^2 + H^2)}. \tag{3}$$

The term V_m is present in both the torques and the inertial term, and will cancel out in (3), indicating that the Mag-μBot's volume does not affect its angular acceleration. However, $J \propto L^5$, while $|\boldsymbol{T}_g| \propto L^4$, and $|\boldsymbol{T}_m| \propto L^3$. This implies $\ddot{\theta} \propto L^{-1}$, which indicates that as the characteristic length of the Mag-μBot increases, it experiences decreased response to high frequency excitations, shown schematically in Fig. 2. This decreased response leads to a reduction in translational velocity by stick-slip motion.

IV. Control of Multiple Mag-μBots

To control a set of k heterogeneous micro-robots, the velocity of each must be determined at various magnetic field pulsing frequencies. The unique velocity response of each micro-robot can then be used to independently address multiple micro-robots.

A. One-Dimensional Control of Multiple Agents

At a particular pulsing frequency f, the translational velocity of all k Mag-μBots is given by $\boldsymbol{v}_f = \begin{bmatrix} v_{1f} & v_{2f} & \dots & v_{kf} \end{bmatrix}^{\mathrm{T}}$. By learning the velocity response for a number of frequencies, a velocity matrix can be constructed, where each column corresponds to the robots' velocity response to a single frequency, $\boldsymbol{v}_f$. For a subset n of the n_a available frequency choices, this velocity matrix is

$$\boldsymbol{\mathcal{V}} = \begin{pmatrix} v_{11} & v_{12} & \dots & v_{1n} \\ v_{21} & v_{22} & \dots & v_{2n} \\ \vdots & \vdots & \ddots & \vdots \\ v_{k1} & v_{k2} & \dots & v_{kn} \end{pmatrix}.$$

A magnetic driving field sequentially pulsed at each of the n frequencies can be applied to the micro-robots for a time given by the vector $\boldsymbol{t} = \begin{bmatrix} t_1 & t_2 & \dots & t_n \end{bmatrix}^{\mathrm{T}}$, where elements correspond to the time spent at each of the n frequency choices. When the fields are applied in sequence for times given by $\boldsymbol{t}$, the robots will move a distance

$$\boldsymbol{x} = \boldsymbol{\mathcal{V}}\boldsymbol{t}. \tag{4}$$

Negative elements in $\boldsymbol{t}$ indicate that the horizontal component of the directing field is negative for that frequency setting such that all micro-robots move in the negative direction.

If a motion $\boldsymbol{x}$ of all micro-robots is desired, this can be achieved by solving for $\boldsymbol{t}$:

$$\boldsymbol{t} = \boldsymbol{\mathcal{V}}^{-1}\boldsymbol{x}. \tag{5}$$

This equation is valid for the case $k = n$ ($\boldsymbol{\mathcal{V}}$ is a square matrix). If $n > k$ (more field choices than robots), one possible solution is found using the Moore-Penrose pseudo-inverse:

$$\boldsymbol{t} = \boldsymbol{\mathcal{V}}^{+}\boldsymbol{x}. \tag{6}$$

This solution minimizes the vector length of $\boldsymbol{t}$, which results in a good solution (but not the optimal solution, which would minimize the Manhattan length of $\boldsymbol{t}$ [22]). Solutions to both (5) and (6) can be found only if the rank r of $\boldsymbol{\mathcal{V}}$ satisfies $r \geq k$. That is, the vectors $\boldsymbol{v}_f$ must span the space $\mathbb{R}^k$. If this is true, any goal positions $\boldsymbol{x}$ can be achieved, including the counter-intuitive cases where the micro-robots' net motions are in opposite directions or where one micro-robot remains stationary while others move. This second case is shown schematically in Fig. 3(a), where two micro-robots are moved to goal positions $\boldsymbol{x} = \begin{bmatrix} g_1 & g_2 \end{bmatrix}^{\mathrm{T}}$ by applying fields for times according to $\boldsymbol{t} = \begin{bmatrix} t_1 & t_2 \end{bmatrix}^{\mathrm{T}}$.

Because position error is introduced each time the pulsing frequency is changed, it is desired to minimize n, the number of frequencies, used. The smallest number of fields which can span $\mathbb{R}^k$ is $n = k$, the number of robots. Therefore, k

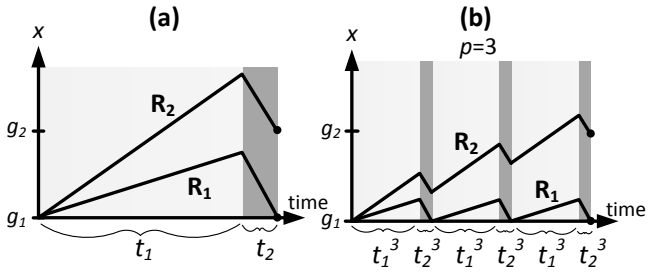

Fig. 3. An example of sequential field applications using two micro-robots ($k = n = 2$). (a) Fields 1 and 2 are applied for the times given by $\boldsymbol{t}$. R_1 and R_2 reach their goal positions g_1 and g_2 in time $t_1 + t_2$. (b) The same fields are applied three times over, for one-third the time ($p = 3$). The same goal displacements are reached in the same time, but the paths more closely resemble direct paths. The same control method can be used for any number of robots.

frequency choices are chosen from the n_a available frequency choices. To find the optimal frequency choices for a desired goal displacement $\boldsymbol{x}$, we minimize the total time, $\sum_{i=1}^{n} |\boldsymbol{t}_i|$. The fields which achieve this minimum value are found by a brute force search over all possible combinations of field choices. Although this optimization method is viable for small numbers of robots, as k and n increase, this search (which requires approximately $\frac{k^3 n!}{k!(n-k)!}$ multiplications) becomes prohibitively expensive and a more efficient optimization routine should be used.

Due to the linear nature of the system, the application of pulsing frequencies for the times given by (5) can be performed in any order. Furthermore, as shown in Fig. 3(b), by sequentially applying pulsing frequencies for time $\boldsymbol{t}^p = \frac{1}{p}\boldsymbol{t}$ (where p is an integer), p times over, the same distance $\boldsymbol{x}$ may be covered, but the path of the robots will approach that of a direct path as p increases. If p is chosen such that the total time per cycle

$$\tau = \sum_{i=1}^{n} |\boldsymbol{t}_i^p| \tag{7}$$

is small, the robots appear to follow straight paths to their destinations. This is useful for any task where the positions of the robots during travel are important, such as in collision avoidance, object manipulation, or when operating in a confined space. The switching frequency f_s of this behavior is given by the inverse of the switching period τ:

$$f_s = \frac{1}{\tau} = \left(\sum_{i=1}^{n} |\boldsymbol{t}_i^p| \right)^{-1}. \tag{8}$$

While theoretically, any switching frequency f_s can be used, there are practical limits. Each time the system switches the motion direction, the micro-robots must all rotate, which induces additional position errors because the micro-robots do not rotate about their centers.

B. Two-Dimensional Control of Multiple Agents

The desired motions of all micro-robots in two dimensions are initially defined by the two vectors $\boldsymbol{x}$ and $\boldsymbol{y}$, representing the displacement components of each robot in the global orthogonal $(\boldsymbol{i}, \boldsymbol{j})$ coordinate system. These components can be combined into a $k \times 2$ matrix $\mathsf{X} = \begin{bmatrix} \boldsymbol{x} & \boldsymbol{y} \end{bmatrix}$. Because the micro-robots can move in any direction in the plane, a new coordinate system can be defined. As shown in Fig. 4(a), the directions $\boldsymbol{e}_a$ and $\boldsymbol{e}_b$ can be arbitrarily chosen, for which the motion coordinates of the desired motions in this frame $\boldsymbol{\alpha} = \begin{bmatrix} \alpha_1 & \alpha_2 & \cdots & \alpha_k \end{bmatrix}^{\mathrm{T}}$ and $\boldsymbol{\beta} = \begin{bmatrix} \beta_1 & \beta_2 & \cdots & \beta_k \end{bmatrix}^{\mathrm{T}}$ can be found, representing the coordinates in the $\boldsymbol{e}_a$ and $\boldsymbol{e}_b$ directions, respectively. The relation between $(\boldsymbol{e}_a, \boldsymbol{e}_b)$ coordinates $\begin{bmatrix} \boldsymbol{\alpha} & \boldsymbol{\beta} \end{bmatrix}$ and global $(\boldsymbol{i}, \boldsymbol{j})$ coordinates X is

$$\mathsf{X} = \begin{bmatrix} \boldsymbol{\alpha} & \boldsymbol{\beta} \end{bmatrix} \mathsf{E} \tag{9}$$

where $\mathsf{E} = \begin{bmatrix} \boldsymbol{e}_a^{\mathrm{T}} \\ \boldsymbol{e}_b^{\mathrm{T}} \end{bmatrix}$. Solving (9) for $\begin{bmatrix} \boldsymbol{\alpha} & \boldsymbol{\beta} \end{bmatrix}$ and combining with (5) yields

$$\mathsf{T} = \boldsymbol{\mathcal{V}}^{-1} \mathsf{X} \mathsf{E}^{-1} \tag{10}$$

where $\mathsf{T} = \begin{bmatrix} {}^{\boldsymbol{e}_a}\boldsymbol{t} & {}^{\boldsymbol{e}_b}\boldsymbol{t} \end{bmatrix}$ contains the time vectors associated with the $\boldsymbol{e_a}$ and $\boldsymbol{e_b}$ directions. Using (10), arbitrary motions of all micro-robots in two dimensions can be achieved by first moving all micro-robots to their $\boldsymbol{e}_a$ coordinates $\boldsymbol{\alpha}$ using one dimensional motion with times given by ${}^{\boldsymbol{e}_a}\boldsymbol{t}$, and then to their $\boldsymbol{e}_b$ coordinates $\boldsymbol{\beta}$ using one dimensional motion with times given by ${}^{\boldsymbol{e}_b}\boldsymbol{t}$. This solution is shown in Fig. 4(b).

As any linearly independent unit vectors $\boldsymbol{e}_a$ and $\boldsymbol{e}_b$ can be used in the solution of (10), an optimal choice can be found by minimizing the total time $\sum_{k=1}^{n} (|{}^{\boldsymbol{e}_a}\boldsymbol{t}_k| + |{}^{\boldsymbol{e}_b}\boldsymbol{t}_k|)$. Additionally, by applying ${}^{\boldsymbol{e}_a}\boldsymbol{t}$ and ${}^{\boldsymbol{e}_b}\boldsymbol{t}$ in a mixed fashion (with $\boldsymbol{e}_a$ and $\boldsymbol{e}_b$ motion alternated in time), all robots follow straighter paths in 2D to their destinations, as in Fig. 4(c).

V. Experiments

A. Velocity Characterization

For each velocity experiment, ten trials were performed where a Mag-μBot was translated by autonomous computer servoing for 1.5 s. A particle filter algorithm based on the gradient of the image was used to automatically track the positions of the micro-robots in real-time at over 70 frames/s. The position differentiated over time is used to calculate the average velocity of a micro-robot over the entire 1.5 s trial. Across a travel distance of about 5 mm, a positioning error of 1-2 pixels (about 60 μm) results in a 0.5% error in measured velocity. Velocity standard deviation is also calculated over the ten trials. All experiments were performed on a glass surface under water, which is a low surface adhesion environment [20].

1) Robots with Different Aspect Ratios: Three hard magnetic Mag-μBots with similar effective magnetization but different aspect ratios were used, with the expectation that the Mag-μBot with the lowest aspect ratio (and thus the lowest rotational inertia) would exhibit roll-off behavior at the highest frequencies. The Mag-μBot magnetizing fields were imposed in an iterative increasing/decreasing process in a vibrating sample magnetometer (model DMS 1660) until similar values were achieved for each robot. Because the effective magnetization $\boldsymbol{M}_{\text{eff}}$ cannot be measured directly, it is calculated from the magnetic moment ($\boldsymbol{M}_{\text{eff}} = \boldsymbol{m}/V_m$).

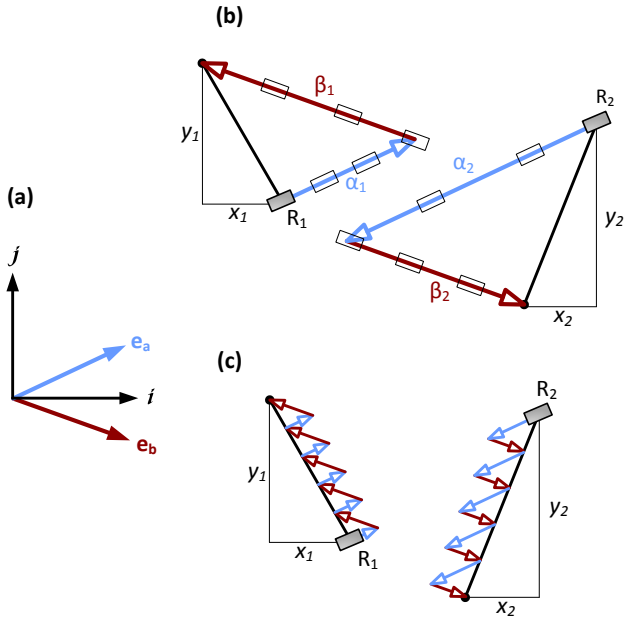

Fig. 4. Two dimensional control of two micro-robots, R_1 and R_2. (a) The global ($\boldsymbol{i}$, $\boldsymbol{j}$) and the arbitrarily chosen ($\boldsymbol{e_a}$, $\boldsymbol{e_b}$) coordinate systems. (b) The robots move sequentially from their initial positions to the points given by $\boldsymbol{x}$ and $\boldsymbol{y}$. They move in sequence along the $\boldsymbol{e}_a$ and the $\boldsymbol{e}_b$ directions for distances $\boldsymbol{\alpha}$ and $\boldsymbol{\beta}$, respectively, as calculated in (10). (c) The same $\boldsymbol{x}$ and $\boldsymbol{y}$ trajectories are achieved, but here, motion in the $\boldsymbol{e}_a$ and $\boldsymbol{e}_b$ directions is quickly alternated, resulting in a path which more closely resembles that of a straight line. The same control method can be used for any number of micro-robots.

TABLE I
LENGTH-VARYING MAG-μBOT PROPERTIES.

Robot	L (μm)	W (μm)	H (μm)	Moment (mEMU)	$\boldsymbol{M}_{\text{eff}}$ (kA/m)
R_1	328	154	91	0.24	50.6
R_2	502	166	84	0.34	49.0
R_3	840	178	69	0.52	50.2

For all Mag-μBots, the magnetization direction is along the reported length direction. Micro-robot properties are given in Table I.

In Fig. 5, a z-directed sawtooth magnetic field waveform with a peak-to-peak amplitude of 1.1 mT and offset of 0.55 mT was used, while the pulsing frequency f was varied for the three Mag-μBots. The x-directed field was held at 1.1 mT. The field magnitude was chosen as the smallest value which results in consistent motion of this micro-robot. The effect of field strength on micro-robot responses is discussed in [15]. To ensure that experimental conditions remain constant, the Mag-μBot is enforced to stay resting on one edge by executing relatively slow turning (10 ms to turn a full circle). Independent velocity responses are seen, where the shortest Mag-μBot's (R_1) velocity did not peak, the medium length Mag-μBot's (R_2) velocity peaked at 120 Hz, while the longest Mag-μBot's (R_3) velocity peaked at 35 Hz. It can be seen that the responses are indeed independent, implying a solution to (5).

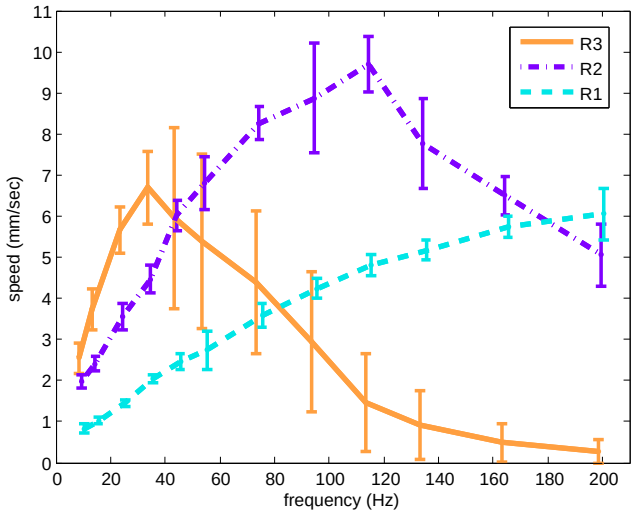

Fig. 5. Experimental velocity responses of three magnetically hard Mag-μBots with varying aspect ratios but similar values of effective magnetization. The maximum field strength was held at 1.1 mT. Geometric and magnetic properties of the Mag-μBots used are listed in Table I. Data points are mean values and error bars represent standard deviations for ten trials.

TABLE II
IDENTICALLY-FABRICATED MAG-μBOT PROPERTIES.

Robot	L (μm)	W (μm)	H (μm)	Moment (mEMU)	$\boldsymbol{M}_{\text{eff}}$ (kA/m)
R_4	608	332	147	2.631	80.9
R_5	609	330	137	3.360	122
R_6	594	342	138	3.190	114

As seen in Fig. 5, depending on the local surface roughness, particulate contamination, and other environmental factors, robot velocity can vary for some operating conditions. However, heterogeneous control of multiple robots can still be accomplished using feedback control to reject these disturbances.

2) Identically-Fabricated Robots: To show that even the small differences due to manufacturing variability can result in independent responses, three identically-fabricated Mag-μBots were used to determine if a group of such "identical" Mag-μBots can be controlled independently. Each robot was magnetized in the same field of 1 T flux density, although variation in magnetization is observed. These micro-robot parameters are given in Table II, with the magnetization direction along the reported length direction.

In Fig. 6, a z-directed sawtooth magnetic field waveform with a peak-to-peak amplitude of 1.6 mT and 0.8 mT offset was used, while f was varied for the three Mag-μBots. The x-directed field was held at 1.6 mT. Because the variation among robots is small, all three lines follow similar but not identical paths. Notice that R_4's effective magnetization $\boldsymbol{M}_{\text{eff}}$ is significantly different than that of R_5 and R_6, but that R_6 is the outlier in Fig. 6. This suggests that here, variability in the velocity response stems primarily from other factors such as small geometric differences between the Mag-μBots. Notice, especially for R_6, that the responses are independent, but to a

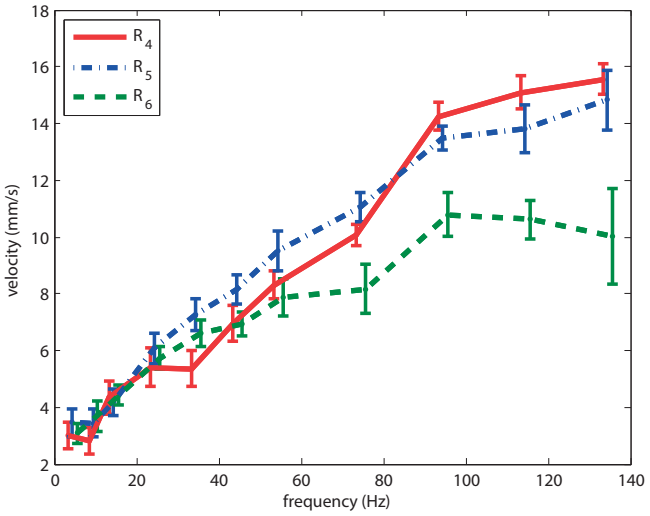

Fig. 6. Experimental velocity responses of three identically-fabricated Mag-μBots with manufacturing variability. The maximum field strength was held at 1.6 mT. Geometric and magnetic properties of the Mag-μBots used are listed in Table II. Data points are mean values and error bars represent standard deviations for ten trials.

lesser degree than the length-varying micro-robots of Fig. 5.

B. Velocity Response Training

To generate the velocity matrix $\boldsymbol{\mathcal{V}}$, mean micro-robot velocity responses are learned by averaging the observed velocity for a specified length of time for each frequency setting. This learning duration influences the accuracy of the learned velocity. The learned velocity values for a single micro-robot at a single field setting are compared to the actual velocity of the robot in Fig. 7. The actual velocity of the robot is determined by averaging the observed velocity over a long period of time (50 s). Position samples, which are differentiated to get velocity, are taken at a frequency of approximately 70 Hz while the micro-robot moves along a square path with edge length of 10 mm. This experiment was performed on micro-robot R_2 at a pulsing frequency of 5 Hz with an average field strength of 3.0 mT. As expected, the relative error decreases with increasing training time, and saturates at around 1.5 s (100 samples) to about 20% relative error. This saturation error represents the inherent stochasticity of Mag-μBot motion, and varies with operating conditions and the micro-robot used.

C. Variance in Velocity Response

Variance in micro-robot velocity has a negative impact on controllability because it induces error to the control times calculated in (5). Because variance in velocity cannot be controlled in experiment for a single micro-robot, a simple kinematic simulation is used which takes empirical mean velocity data and adds a specified velocity error assuming a Gaussian error distribution. This error is given as a percent of mean velocity. The simulated micro-robots perform a one-dimensional motion task (each moving 20 mm in opposite directions), governed by (5), and the time to complete the task is recorded for 300 trials at each standard deviation value.

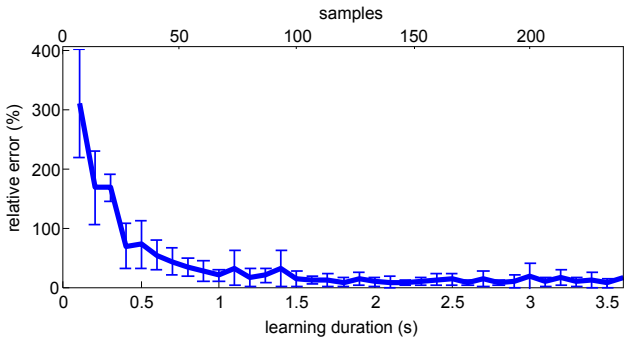

Fig. 7. The effect of velocity response learning time on the accuracy of the learned velocity. Velocity samples are taken at approximately 70 Hz while the micro-robot moves along a square path with edge length of 10 mm. The relative error decreases with increasing training time and saturates at around 1.5 s to about 20% relative error. Error bars represent max and min values for three trials at each data point. This experiment was performed using micro-robot R_2 at a pulsing frequency of 5 Hz with an average field strength of 3.0 mT.

The mean velocity data used is from a set of four identically-fabricated micro-robots, a portion which is shown in Fig. 6.

The simulation moves the micro-robots in time steps of 0.02 s, choosing the optimal frequencies to use in the manner of section IV-A. The position of each micro-robot is incremented using the experimental mean velocity with a random error added each time step assuming a Gaussian distribution. The results, shown in Fig. 8, are for one to four micro-robots, and are normalized by the time to complete the task for one micro-robot with no velocity variance. From the figure, it is noted that the detrimental effect of variance is much more prevalent for larger numbers of micro-robots. For one or two micro-robots ($N = 1$, $N = 2$), the completion time is much less variant with velocity error because the system is less sensitive to these disturbances. However, for more than two micro-robots, the completion time increases quickly with increasing velocity error. This behavior has significant negative implications for the controllability of larger numbers of heterogeneous micro-robots with large velocity variance.

D. Goal Tolerance

A motion task is determined to be complete when all micro-robots are within a tolerance distance δ of their goal positions. The effect of goal tolerance is studied using the kinematic simulation, and results are shown in Fig. 9. The goal tolerance δ is varied between 150 μm and 4500 μm. It can be seen that increasing δ decreases the time to complete the task, especially when the velocity error of the micro-robots is large.

E. Robot Diversity

By altering the difference between a pair of micro-robots, the performance of the pair is affected. Pairs of micro-robots were used with varying length ratios: one very long micro-robot (R_7) was paired with another micro-robot of varying length (R_8–R_{12}) and the time to finish a motion task was recorded, as presented in Fig. 10. Micro-robot dimensions used for this experiment are given in Table III. All six of these micro-robots were magnetized in a field of flux density

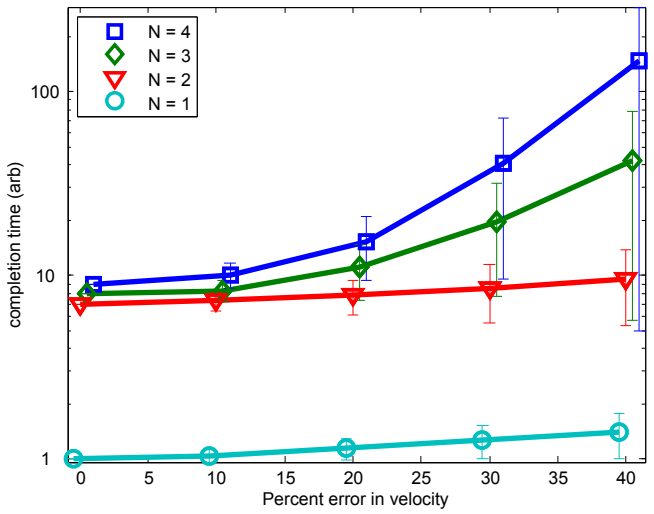

Fig. 8. Simulated effect of velocity error and number of robots on task completion time. The simulated robots perform a one-dimensional motion task (each moving 20 mm in opposite directions) and the time to complete the task is recorded for each velocity error value. Using real mean velocity data from one to four identical Mag-μBots, with deviation replaced. The goal tolerance for each robot is δ =1 mm. Each data point represents the mean of 300 simulation trials, with error bars indicating standard deviation in time. x-axis values are adjusted slightly for visibility.

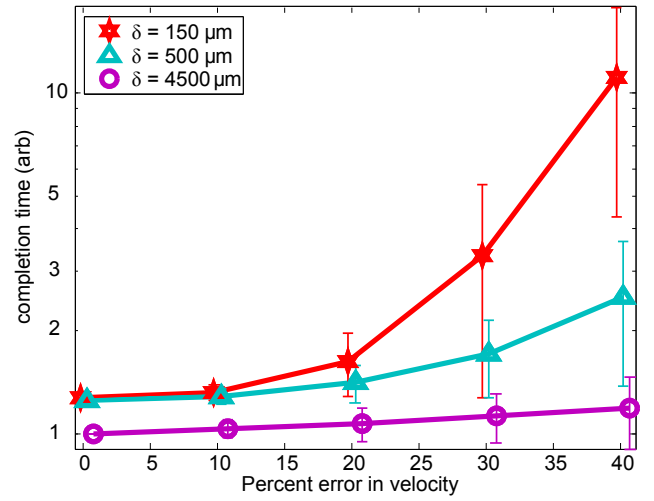

Fig. 9. Simulated effect of velocity error and goal tolerance on task completion time. The three simulated robots perform a one-dimensional motion task (each moving 20 mm in opposite directions) and the time to complete the task is recorded for each velocity error value. Using real mean velocity data from one to four identical Mag-μBots, with deviation replaced. The goal tolerance, δ is varied between 0.150 mm and 4.50 mm.

1 T. As the diversity (length ratio) of the pairs increases, the time to complete the task decreases, but indicates saturation at higher length ratios. These results suggest that while higher length ratios may result in better performance, the change in performance time was not overwhelming.

F. Switching Frequency

As previously discussed, the switching frequency f_s, calculated in (8), effects how straight the paths of the micro-robots are. In Fig. 4, increasing f_s causes the paths to more

TABLE III
MAG-μBOT DIMENSIONS USED FOR DIVERSITY EXPERIMENT

Robot	L (μm)	W (μm)	H (μm)
R_7	1140	207	142
R_8	846	216	133
R_9	718	230	132
R_{10}	563	228	149
R_{11}	402	230	140
R_{12}	252	233	131

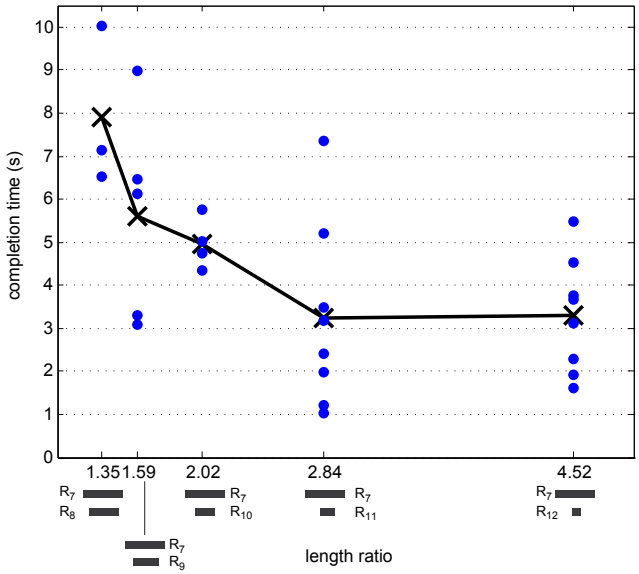

Fig. 10. Effect of micro-robot diversity on task completion time. Pairs of micro-robots were used with varying heterogeneity. One very long micro-robot (R_7) was paired with another robot of varying length (R_8-R_{12}) and the time to finish a motion task was recorded. Black $\times$ markers indicate the mean of the datapoints at each length ratio. Micro-robots are moved in opposite directions for 5 mm, with a tolerance of δ =1.3 mm. Micro-robot properties are given in Table III.

closely resemble straight lines. The frequency of switching was varied in experiment for a pair of micro-robots moving perpendicularly to each other. During this motion, the location of each robot was tracked and the average path error (mean distance from desired path line) was calculated. The average error using micro-robots R_7 and R_{11}, shown in Fig. 11 for various switching frequencies, shows that mid-range frequencies outperform those at higher or lower values. For low switching frequencies, the micro-robot motion in each direction $\boldsymbol{e}_a$ and $\boldsymbol{e}_b$ is exaggerated, leading to large average error. For high switching frequencies, the deviation from the desired path is less. However, each time the system switches direction, all robots must rotate between $\pm\boldsymbol{e}_a$ and $\pm\boldsymbol{e}_b$, which adds error as robots do not rotate about their centers. In this experiment, the available motion directions are constrained to $\angle\boldsymbol{e}_a = 0$ and $\angle\boldsymbol{e}_b = \pi/2$ (perpendicular motions) so that the behavior in each case can be more easily compared without the influence of arbitrary motion directions.

One representative path of the two micro-robots in two

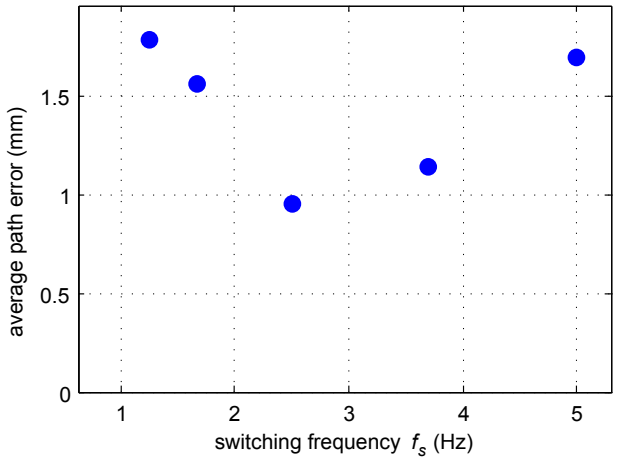

Fig. 11. The frequency of switching was varied for a pair of micro-robots moving perpendicularly to each other. The position error during the task was averaged for five trials at each f_s value, and is plotted here against the switching frequency.

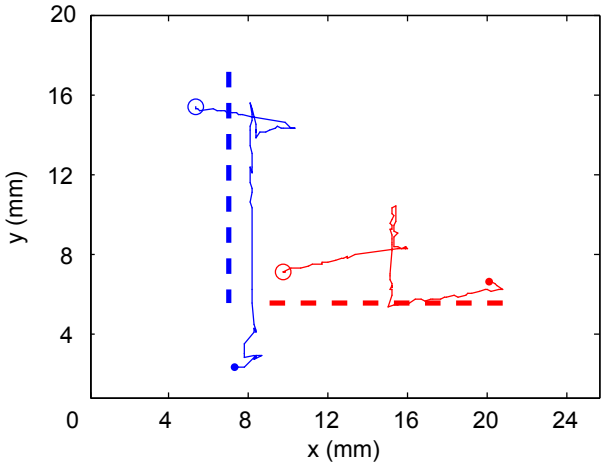

Fig. 12. Representative micro-robot paths in two dimensions, controlled with a switching frequency of $f_s = 1.25$ Hz. The dashed line is the desired trajectory for each robot and the solid line is the actual path. The robots start at the open circles and end at the dots. At this slow switching speed, the segments of straight motion are long, and the micro-robot moves far from the path each time.

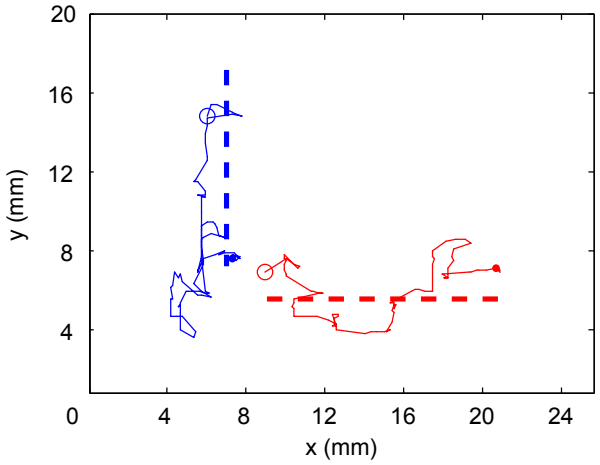

Fig. 13. Representative micro-robot paths in two dimensions, controlled with a switching frequency of $f_s = 5.0$ Hz. The dashed line is the desired trajectory for each robot and the solid line is the actual path. The robots start at the open circles and end at the dots. At this high switching speed, the motion is erratic because each time a direction switch occurs the locations of the micro-robots are perturbed, adding error to the motion.

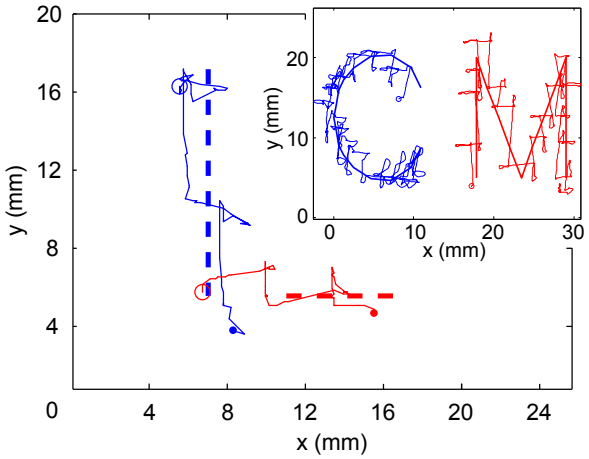

Fig. 14. Representative micro-robot paths in two dimensions, controlled with a switching frequency of $f_s = 2.5$ Hz. The dashed line is the desired trajectory for each robot and the solid line is the actual path. The robots start at the open circles and end at the dots. At this optimal switching speed, the segments of straight motion are medium length, and the average deviation from the desired path is small. The inset shows the micro-robots following a more complex 'CM' path using the same settings.

dimensions is plotted in Figs. 12-14 for different switching frequencies. In Fig. 12 ($f_s = 1.25$ Hz), the switching frequency is too low, resulting in exaggerated motions. The entire motion is completed in 1.5 cycles ($p = 1.5$), each of which can be seen clearly. Although the final displacement is accurate, each robot must deviate significantly from its path each cycle, resulting in large motions perpendicular to the desired paths. In Fig. 13 ($f_s = 5.0$ Hz), the switching frequency is too high and the resulting motion is erratic. Each time a direction switch occurs the locations of the micro-robots are perturbed, adding error to the motion. In this case, these additional errors are a significant portion of the motion. The task is completed here in about 10 cycles ($p = 10$). In the best case of Fig. 14 ($f_s = 2.5$ Hz), each negative aspect is kept to a minimum and the micro-robot stays relatively close to the desired path, completing the task in 2.5 cycles ($p = 2.5$). The inset of Fig. 14 shows the path-following capabilities of the two micro-robots at this pulsing frequency. It is seen that the Mag-μBots follow the complex paths 'C' and 'M' simultaneously within an error bound.

The time to complete the task for each switching frequency is shown in Fig. 15. In general, the results indicate no dependence on the switching frequency. Therefore, f_s can be chosen to limit the average path error without significantly influencing the task completion time.

G. Demonstration

To demonstrate the feasibility of moving multiple Mag-μBots simultaneously, two or three Mag-μBots were positioned using the methods described in section IV. Several video frames from an experiment of two (Fig. 16) or three

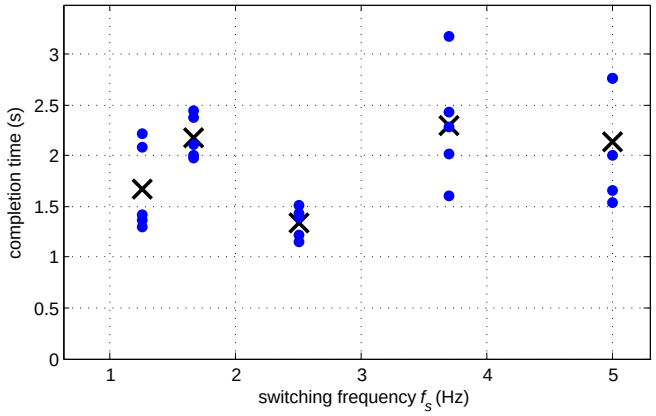

Fig. 15. The frequency of switching was varied for a pair of micro-robots moving perpendicularly to each other. The time to complete the entire task is plotted against the switching frequency. The plot shows that the switching frequency does not have a large effect on the completion time. Black × markers indicate the mean of the five datapoints at each switching frequency.

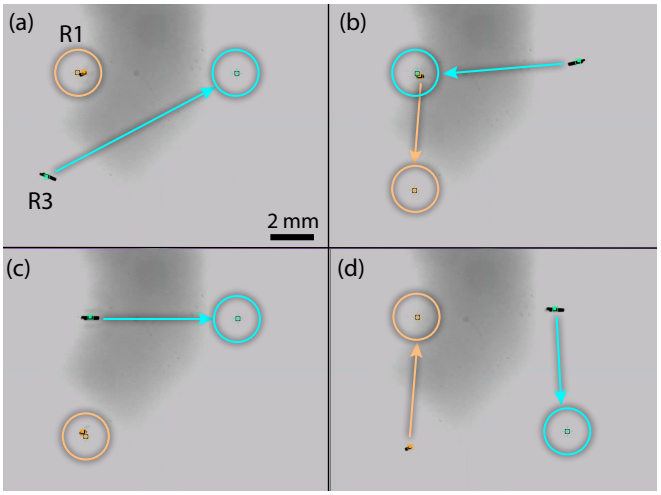

Fig. 16. Frames from a top-view movie showing independent control of two length-varying heterogeneous Mag-μBots, R_1 and R_2, operating in water on a glass surface. The pulsing frequency is chosen from values between 5 and 135 Hz, as in Fig. 5. Goal positions of radius $\delta = 1$ mm are indicated by the circles. Each motion task is complete when all robots lie inside their goal circles. (a) Only R_3 moves. (b) R_1 and R_3 move in perpendicular directions. (c) Only R_3 moves. (d) R_1 and R_3 move in opposite directions. Video available in supplementary materials.

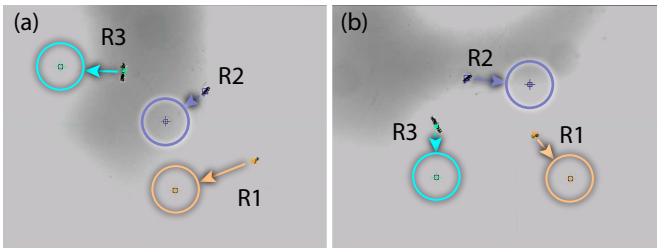

Fig. 17. Frames from a top-view movie showing independent control of three length-varying heterogeneous Mag-μBots, R_1, R_2 and R_3, operating in water on a glass surface. The pulsing frequency is chosen from values between 5 and 135 Hz, as in Fig. 5. Goal positions of radius $\delta = 1$ mm are indicated by the circles. Each motion task is complete when all robots lie inside their goal circles. Video available in supplementary materials.

(Fig. 17) length-varying robots are displayed. Using (10), independent control of each robot is shown in two dimensions, allowing all robots to move to arbitrary final positions. Goal destinations were chosen manually to avoid collisions, with a large goal tolerance of $\delta = 1.0$ mm. to increase experiment speed.

It is noted that control of two micro-robots is much more robust than control of three. With more micro-robots, the system is very sensitive to errors in the learned velocity, but with two micro-robots, large errors can be handled. Failure occurs when one or more micro-robots deviates from its path enough to leave the viewing area or collide with another robot. The completion of the movement task was successful for $\sim 90\%$ of ten trials with two micro-robots but only for $\sim 20\%$ of ten trials with three micro-robots.

Due to even greater sensitivity to error, heterogeneous control of more than three micro-robots has not been achieved. For this to be successful, it may require more accurate velocity learning and the concurrent use of other selection methods such as selection by field strength or by using magnetically hard and soft micro-robots together. By reducing the coupling between the responses, this method could be extended to the control of more micro-robots.

Heterogeneous control of two identically-fabricated micro-robots was also demonstrated. Because the velocity response curves are very similar (see Fig. 6), the micro-robot motion is very sensitive to error, thus it takes over twice as long for the micro-robots to reach their goal positions. This is shown in the supplemental video.

VI. Conclusions

A method for the response learning and motion planning of heterogeneous groups of magnetic micro-robots was demonstrated. In this method, up to three Mag-μBots were controlled in a coupled fashion that allows for independent global positioning of each micro-robot without the use of a specialized operating surface. Geometrically dissimilar Mag-μBots were fabricated so that they responded differently to the actuation magnetic fields. Groups of identically-fabricated micro-robots were also shown to be individually controllable in some cases due to slight fabrication differences. By learning the response of all robots to different pulsing frequencies, positioning to arbitrary goal positions and limited path following was demonstrated. Additionally, operation parameters were studied for 1D and 2D robot control to find the fastest and most accurate conditions. Experimental results validated the theory and motion control of up to three Mag-μBots was shown in two dimensions. It was shown in simulation that simultaneous control of additional micro-robots using the proposed method becomes increasingly sensitive to velocity error in the micro-robot responses. Thus, the control of more than three micro-robots will require reduced coupling between micro-robots.

Future works will further incorporate vision, path planning, and appropriate selection and control algorithms to autonomously control heterogeneous sets of Mag-μBots to perform tasks such as team manipulation of micro-scale objects. In addition, expanding heterogeneous control of micro-robots to three dimensions will be explored.

ACKNOWLEDGMENT

The authors would like to thank the NanoRobotics Laboratory members for their support and suggestions. This work is supported by the National Science Foundation CAREER award program (NSF IIS-0448042) and the NSF Graduate Research Fellowship.

REFERENCES

[1] B. Donald, C. Levey, and I. Paprotny, "Planar microassembly by parallel actuation of MEMS microrobots," *J. Microelectromech. Sys.*, vol. 17, pp. 789–808, 2008.

[2] M. Sakar, E. B. Steager, A. A. Juliusz, M. Kim, V. Kumar, and G. J. Pappas, "Biosensing and actuation for microbiorobots," in *IEEE Int. Conf. Rob. Autom.*, Anchorage, AK, 2010, pp. 3141–3146.

[3] D. R. Frutiger, K. Vollmers, B. E. Kratochvil, and B. J. Nelson, "Small, fast, and under control: Wireless resonant magnetic micro-agents," *Int. J. Rob. Res.*, vol. 29, pp. 613–636, 2009.

[4] L. Zhang, J. Abbott, L. Dong, B. Kratochvil, D. Bell, and B. Nelson, "Artificial bacterial flagella: Fabrication and magnetic control," *App. Phy. Lett.*, vol. 94, no. 064107, 2009.

[5] A. Yamazaki, M. Sendoh, K. Ishiyama, K. I. Arai, R. Kato, M. Nakano, and H. Fukunaga, "Wireless micro swimming machine with magnetic thin film," *J. Mag. and Mag. Mat.*, vol. 272-276, pp. 1741–1742, 2004.

[6] C. Pawashe, S. Floyd, and M. Sitti, "Modeling and experimental characterization of an untethered magnetic micro-robot," *Int. J. Rob. Res.*, vol. 28, pp. 1077–1094, 2009.

[7] A. Ghosh and P. Fischer, "Controlled propulsion of artificial magnetic nanostructured propellers," *Nano Lett.*, vol. 9, pp. 2243–2245, 2009.

[8] H. Maruyama, T. Fukuda, and F. Arai, "Laser manipulation and optical adhesion control of a functional gel-microtool for on-chip cell manipulation," in *IEEE Int. Conf. Rob. Auton. Sys.*, St. Louis, MO, 2009, pp. 1413–1418.

[9] O. Sul, M. Falvo, R. Taylor, S. Washburn, and R. Superfine, "Thermally actuated untethered impact-driven locomotive microdevices," *App. Phys. Lett.*, vol. 89, no. 203512, 2006.

[10] A. Solovev, Y. Mei, E. Urena, G. Huang, and O. Schmidt, "Catalytic microtubular jet engines self-propelled by accumulated gas bubbles," *Small*, vol. 5, pp. 1688–1692, 2009.

[11] S. Martel, M. Mohammadi, O. Felfoul, Z. Lu, and P. Pouponneau, "Flagellated magnetotactic bacteria as controlled MRI-trackable propulsion and steering systems for medical nanorobots operating in the human microvasculature," *Int. J. Rob. Res.*, vol. 28, no. 571-582, 2009.

[12] B. Behkam and M. Sitti, "Bacterial flagella-based propulsion and on/off motion control of microscale objects," *App. Phys. Lett.*, vol. 90, no. 023902, 2007.

[13] B. Kratochvil, D. Frutiger, K. Vollmers, and B. Nelson, "Visual servoing and characterization of resonant magnetic actuators for decoupled locomotion of multiple untethered mobile microrobots," in *IEEE Int. Conf. Rob. Autom.*, Kobe, Japan, 2009, pp. 1010–1015.

[14] T. Bretl, "Control of many agents using few instructions," in *Proc. Robot.: Sci. Syst. Conf*, 2007.

[15] S. Floyd, E. Diller, C. Pawashe, and M. Sitti, "Control methodologies for a heterogeneous group of untethered magnetic micro-robots," *Int. J. Rob. Res.*, available online March 2011.

[16] E. Diller, S. Floyd, C. Pawashe, and M. Sitti, "Control of multiple heterogeneous magnetic micro-robots on non-specialized surfaces," in *IEEE Int. Conf. Rob. Autom.*, Shanghai, China, May 2011, pp. 115–120.

[17] C. Pawashe, S. Floyd, and M. Sitti, "Multiple magnetic microrobot control using electrostatic anchoring," *App. Phys. Lett.*, vol. 94, no. 164108, 2009.

[18] S. Floyd, C. Pawashe, and M. Sitti, "Microparticle manipulation using multiple untethered magnetic microrobots on an electrostatic surface," in *IEEE Int. Conf. Rob. Auton. Sys.*, St. Louis, Missouri, 2009, pp. 528–533.

[19] M. Imbaby, K. Jiang, and I. Chang, "Net shape fabrication of stainless-steel micro machine components from metallic powder," *J. Micromech. and Microeng.*, vol. 18, pp. 115 018–115 025, 2008.

[20] S. Floyd, C. Pawashe, and M. Sitti, "Two-dimensional contact and non-contact micro-manipulation in liquid using an untethered mobile magnetic micro-robot," *IEEE Trans. Rob.*, vol. 25, pp. 1332–1342, 2009.

[21] O. Cugat, J. Delamare, and G. Reyne, "Magnetic micro-actuators and systems (MAGMAS)," *IEEE Trans. Magn.*, vol. 39, no. 6, pp. 3607 – 3612, 2003.

[22] V. Chepoi, K. Nouioua, and Y. Vaxs, "A rounding algorithm for approximating minimum manhattan networks," *Theor. Comp. Sci.*, vol. 390, no. 1, pp. 56 – 69, 2008.

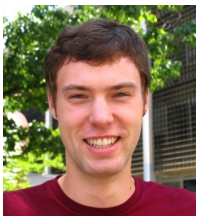

Eric Diller (S'10) received the B.S. and M.S. degrees in mechanical engineering from Case Western Reserve University in Cleveland, OH, in 2009. He is currently a Ph.D. candidate in mechanical engineering at Carnegie Mellon University. His research interests include magnetic actuation, microscale manipulation, and biologically-inspired systems.

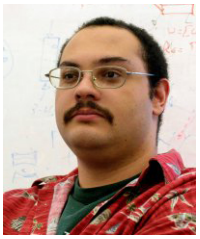

Steven Floyd (S'04-M'11) received the B.S. degree in mechanical engineering (*summa cum laude*) from Washington University in St. Louis, St. Louis, MO, in 2005 and the M.S. and Ph.D. degrees in mechanical engineering from Carnegie Mellon University, Pittsburgh, PA, in 2008 and 2010, respectively. He is at Areté Associates since 2010. His research interests include robotic design, MEMS, analog electronics design, and magnetic power transfer and actuation.

Dr. Floyd received the National Science Foundation Graduate Research Fellowship (2005), the second prize in the World RoboCup Nanogram Demonstration (2007), and the best paper award at IEEE IROS (2009).

Chytra Pawashe received the B.S., M.S., and Ph.D. degrees in mechanical engineering from Carnegie Mellon University, Pittsburgh, PA, USA, in 2006, 2008, and 2010 respectively. He is at Intel Corporation since 2011. His research interests include micro/nanoscale manipulation and assembly, controls and automation, and MEMS/NEMS.

Dr. Pawashe received the second prize in the World RoboCup Nanogram Demonstration (2007), and the best paper award at IEEE IROS (2009).

Metin Sitti Metin Sitti (S'94-M'00-SM'08) received the B.Sc. and M.Sc. degrees in electrical and electronics engineering from Bogazici University, Istanbul, Turkey, in 1992 and 1994, respectively, and the Ph.D. degree in electrical engineering from the University of Tokyo, Tokyo, Japan, in 1999. He was a research scientist at University of California at Berkeley during 1999-2002. He is currently a professor in the Department of Mechanical Engineering and Robotics Institute at Carnegie Mellon University. He is the director of the NanoRobotics Lab and Center for Bio-Robotics. His research interests include micro/nanorobotics, bio-inspired materials and miniature mobile robots, and micro/nanomanipulation. He received the SPIE Nanoengineering Pioneer Award in 2011. He was appointed as the Adamson Career Faculty Fellow during 2007-2010. He was the Vice President of the Technical Activities in the IEEE Nanotechnology Council during 2008-2010. He was elected as the Distinguished Lecturer of the IEEE Robotics and Automation Society for 2006-2008. He received the National Science Foundation CAREER award and Struminger award in 2005. He received the Best Paper Award in the IEEE/RSJ International Conference on Intelligent Robots and Systems in 2009 and 1998, the second prize in the World RoboCup Nanogram Demonstration League in 2007 and 2010, the Best Biomimetics Paper Award in the IEEE Robotics and Biomimetics Conference in 2004, and the Best Video Award in the IEEE Robotics and Automation Conference in 2002. He is the co-editor-in-chief of Journal of Micro/Nano-Mechatronics and an associate editor for IEEE Trans. on Robotics.